On Pairing Glues in Strongly Correlated Superconductors

Frontier of Superconducting Phenomena

Heavy-electrons systems

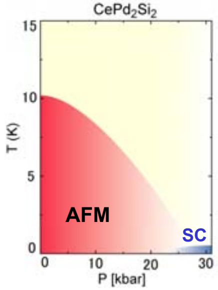

Organic conductors

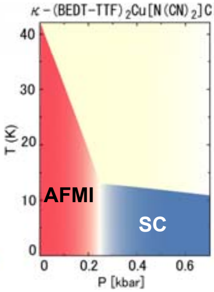

High-T$_c$ copper oxides

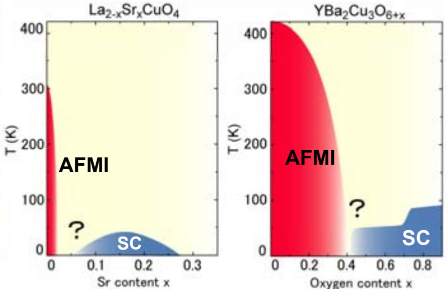

Nearly localized f-electrons

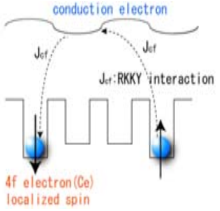

Half-field $p_\pi$bands

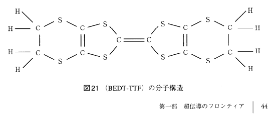

Strongly- Correlated Electrons Systems

Half-filled 3d bands

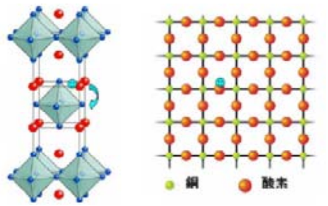

CuO$_2$面

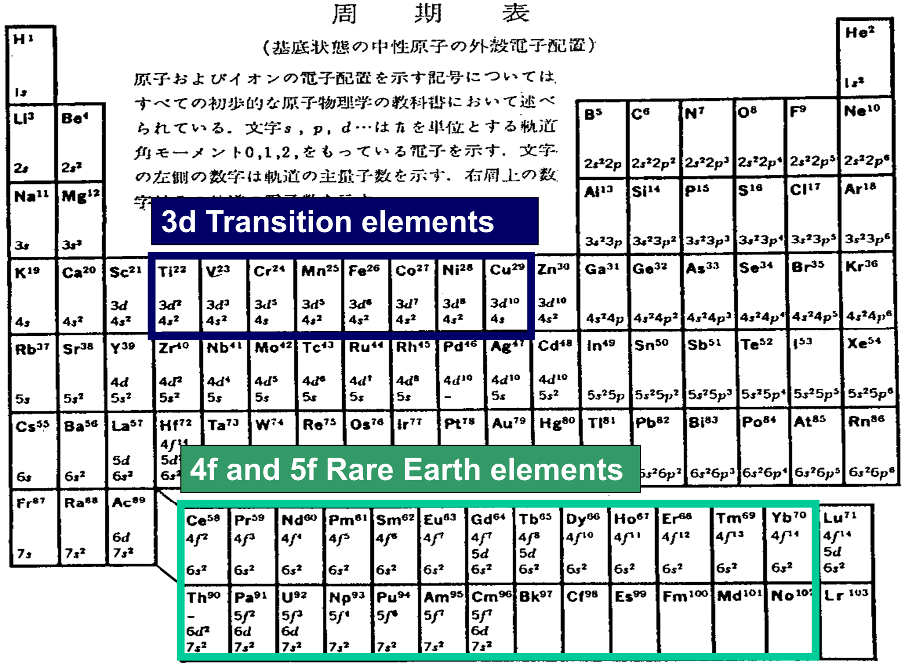

周　期　表

（基底状態の中性原子の外殻電子配置）

原子およびイオンの電子配置を示す記号については，すべての初歩的な原子物理学の教科書において述べられている．文字 s，p，d…は ħ を単位とする軌道角モーメント0,1,2,をもっている電子を示す．文字の左側の数字は軌道の主量子数を示す．右肩上の数字

3d Transition elements

4f and 5f Rare Earth elements

H^1 $1s$																	He^2 $1s^2$
Li^3 $2s$	Be^4 $2s^2$											B^5 $2s^22p$	C^6 $2s^22p^2$	N^7 $2s^22p^3$	O^8 $2s^22p^4$	F^9 $2s^22p^5$	Ne^{10} $2s^22p^6$
Na^{11} $3s$	Mg^{12} $3s^2$											Al^{13} $3s^23p$	Si^{14} $3s^23p^2$	P^{15} $3s^23p^3$	S^{16} $3s^23p^4$	Cl^{17} $3s^23p^5$	Ar^{18} $3s^23p^6$
K^{19} $4s$	Ca^{20} $4s^2$	Sc^{21} $3d$ $4s^2$	Ti^{22} $3d^2$ $4s^2$	V^{23} $3d^3$ $4s^2$	Cr^{24} $3d^5$ $4s$	Mn^{25} $3d^5$ $4s^2$	Fe^{26} $3d^6$ $4s^2$	Co^{27} $3d^7$ $4s^2$	Ni^{28} $3d^8$ $4s^2$	Cu^{29} $3d^{10}$ $4s$	Zn^{30} $3d^{10}$ $4s^2$	Ga^{31} $4s^24p$	Ge^{32} $4s^24p^2$	As^{33} $4s^24p^3$	Se^{34} $4s^24p^4$	Br^{35} $4s^24p^5$	Kr^{36} $4s^24p^6$
Rb^{37} $5s$	Sr^{38} $5s^2$	Y^{39} $4d$ $5s^2$	Zr^{40} $4d^2$ $5s^2$	Nb^{41} $4d^4$ $5s$	Mo^{42} $4d^5$ $5s$	Tc^{43} $4d^6$ $5s$	Ru^{44} $4d^7$ $5s$	Rh^{45} $4d^8$ $5s$	Pd^{46} $4d^{10}$ –	Ag^{47} $4d^{10}$ $5s$	Cd^{48} $4d^{10}$ $5s^2$	In^{49} $5s^25p$	Sn^{50} $5s^25p^2$	Sb^{51} $5s^25p^3$	Te^{52} $5s^25p^4$	I^{53} $5s^25p^5$	Xe^{54} $5s^25p^6$
Cs^{55} $6s$	Ba^{56} $6s^2$	La^{57} $5d$ $6s^2$	Hf^{72} $4f^{14}$ $5d$ $6s$	Ta^{73}	W^{74}	Re^{75}	Os^{76}	Ir^{77}	Pt^{78}	Au^{79}	Hg^{80}	Tl^{81}	Pb^{82} $6s^26p^2$	Bi^{83} $6s^26p^3$	Po^{84} $6s^26p^4$	At^{85} $6s^26p^5$	Rn^{86} $6s^26p^6$
Fr^{87} $7s$	Ra^{88} $7s^2$	Ac^{89} $6d$ $7s^2$															

Ce^{58} $4f^2$ $6s^2$	Pr^{59} $4f^3$ $6s^2$	Nd^{60} $4f^4$ $6s^2$	Pm^{61} $4f^5$ $6s^2$	Sm^{62} $4f^6$ $6s^2$	Eu^{63} $4f^7$ $6s^2$	Gd^{64} $4f^7$ $5d$ $6s^2$	Tb^{65} $4f^8$ $5d$ $6s^2$	Dy^{66} $4f^{10}$ $6s^2$	Ho^{67} $4f^{11}$ $6s^2$	Er^{68} $4f^{12}$ $6s^2$	Tm^{69} $4f^{13}$ $6s^2$	Yb^{70} $4f^{14}$ $6s^2$	Lu^{71} $4f^{14}$ $5d$ $6s^2$
Th^{90} – $6d^2$ $7s^2$	Pa^{91} $5f^2$ $6d$ $7s^2$	U^{92} $5f^3$ $6d$ $7s^2$	Np^{93} $5f^4$ $7s^2$	Pu^{94} $5f^6$ $7s^2$	Am^{95} $5f^7$ $7s^2$	Cm^{96} $5f^7$ $6d$ $7s^2$	Bk^{97}	Cf^{98}	Es^{99}	Fm^{100}	Md^{101}	No^{102}	Lr^{103}

Effective atomic potentials for Ce and U

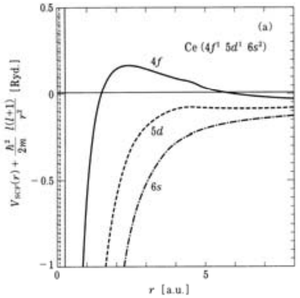

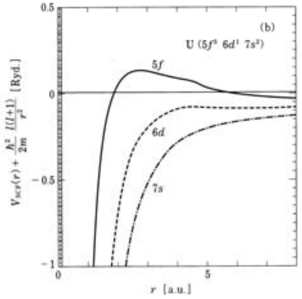

$$\left[-\frac{d^2}{dr^2}-\frac{2}{r}\frac{d}{dr}+U(r)+\frac{l(l+1)}{r^2}\right]\psi=k^2\psi,$$

$$U(r)=\frac{2m}{\hbar^2}V(r),$$

$$\varepsilon=\frac{\hbar^2k^2}{2m}.$$

Anderson Hamiltonian in Strongly Correlated systems

Radial distributions of wave functions of Ce and U

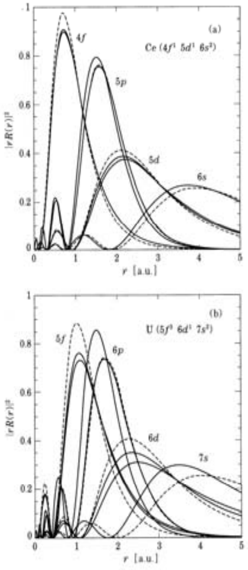

$$\mathscr{H} = \sum_k \sum_\sigma \varepsilon_k c^\dagger_{k\sigma} c_{k\sigma} + \sum_\sigma E_f f^\dagger_\sigma f_\sigma + U n_{f\uparrow} n_{f\downarrow} + \frac{1}{\sqrt{N_0}} \sum_k \sum_\sigma \left(V_{fk} f^\dagger_\sigma c_{k\sigma} + V_{kf} c^\dagger_{k\sigma} f_\sigma \right)$$

Hybridization term in Anderson Hamiltonian

$$\left\langle \frac{1}{\sqrt{\Omega}} e^{i\mathbf{k}\cdot\mathbf{r}} \right| H \left| u_{k_0} Y_{lm} \right\rangle$$

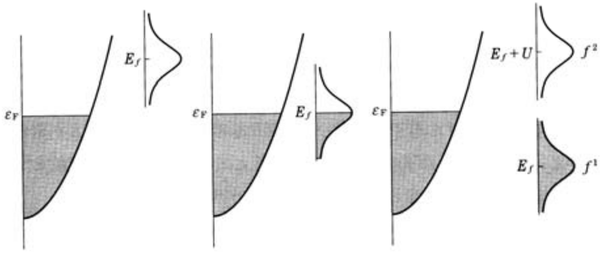

(a) $E_f - \varepsilon_F \gg \Delta$　(b) 価数揺動レジーム　(c) 近藤レジーム

Heavy-Electrons Compounds

RKKY interaction

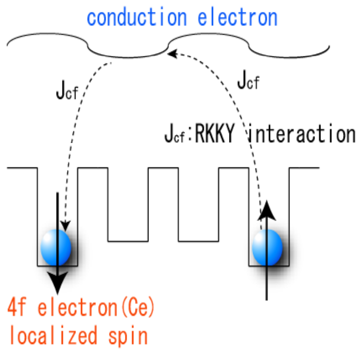

Antiferromagnetic state

Spin quenching (Kondo) effect

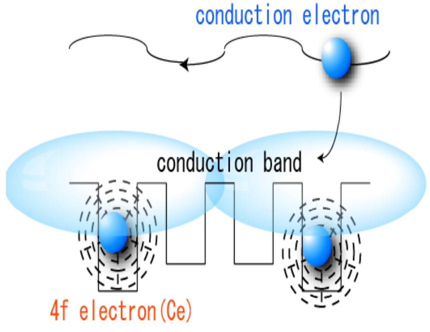

Heavy - Fermi liquid

$$\mathcal{H} = \sum_{k\sigma} \varepsilon_k a^\dagger_{k\sigma} a_{k\sigma} + J_K \sum_i \vec{\sigma}\cdot\vec{S}_i + J_{RKKY} \sum_{\langle ij \rangle} \vec{S}_i \cdot \vec{S}_j$$

$J_K \sim |V|^2/U$　　$U \to$ large (Coulomb repulsion)

$T > J_K/k_B$

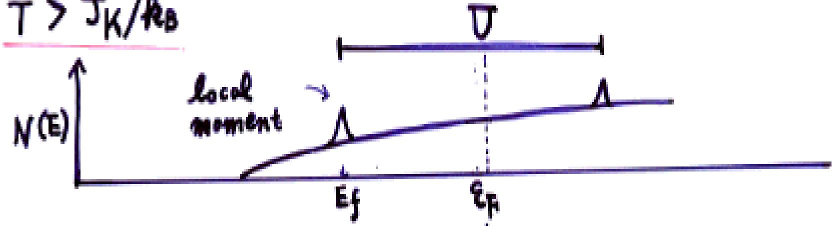

$T \ll J_K/k_B$

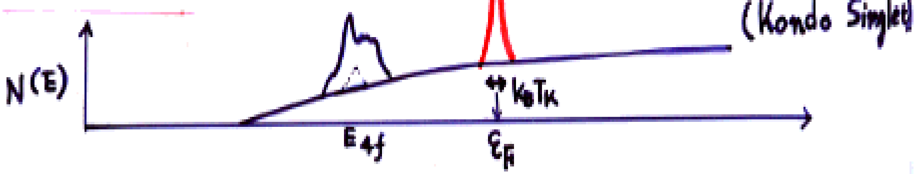

Characteristic Energy Scales in Heavy- Electrons Systems

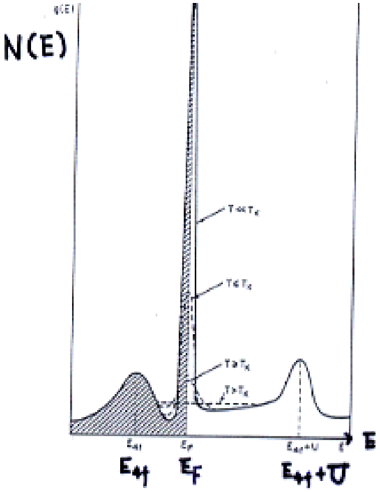

$$J_K \simeq \frac{V_{sf}^2}{E_F - E_{4f}} \sim 1 - 10 meV$$

$$T_K \simeq T_F \exp\left[-\frac{1}{N_c(E_F) J_K}\right] \sim 10 - 100K$$

$$J_{RKKY} \simeq \frac{J_K^2}{E_F}$$

$$N(E_F) = \frac{3 N_A}{\hbar^2 k_F^2} \cdot m^*$$

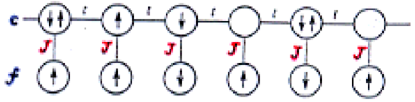

Experimental evidences of heavy electrons

- Specific Heat

$$C = \frac{\pi^2 k_B^2}{3}\rho(E_F)\cdot T = \gamma T$$

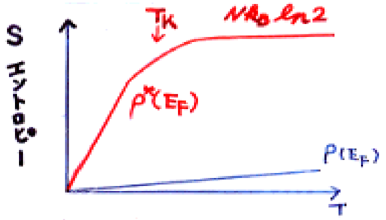

Ce, U Compounds

$\gamma \approx 1000\,\mathrm{mJ/mole\,K^2}$

Free Electron

$\gamma_0 \simeq 1\,\mathrm{mJ/mole\cdot K^2}$

- Susceptibility

$F = E - TS$, S: Entropy

$\chi = \mu_B^2\,\rho(E_F)$

F: Free energy

$\chi = (1\sim5)\times10^{-2}$ emu/mole

$\chi_0 = 1.2\times10^{-5}$ emu/moleK²

$$\rho(E_F) = \frac{3N}{2E_F} = \frac{3N}{\hbar^2 k_F^2}\,m$$

$m^* \approx 1000\,m_0$ ← 重い電子系 Heavy Electron

Magnetic state of Ce^{3+} ($4f^1$) and U^{4+} ($5f^2$)

$4f^1$: S=1/2, L=3, J=3-1/2=5/2

$5f^2$: S=1, L=5, J=5-1=4

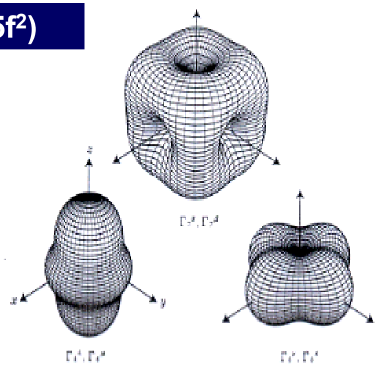

2-6図 Ce^{3+} イオンの立方晶での空間電荷分布

		Spin-Orbit	Crystal Field
Ce 化合物	Ce^{3+} $(4f^1)$	$J=\frac{5}{2}$	$\tau=\frac{1}{2}$
			hybridization
U 化合物	U^{4+} $(5f^2)$	$J=4$	$S=\frac{1}{2}$?

Cubic crystal field effect for $J = 5/2$ ⟹

$$|\Gamma_8^1\rangle = \sqrt{\frac{5}{6}}\left|\frac{5}{2}\right\rangle + \frac{1}{\sqrt{6}}\left|-\frac{3}{2}\right\rangle$$

$$|\Gamma_8^2\rangle = \sqrt{\frac{5}{6}}\left|-\frac{5}{2}\right\rangle + \frac{1}{\sqrt{6}}\left|\frac{3}{2}\right\rangle$$

$$|\Gamma_8^3\rangle = \left|\frac{1}{2}\right\rangle$$

$$|\Gamma_8^4\rangle = \left|-\frac{1}{2}\right\rangle$$

$(1/T_1T) \propto N^*(E_F)^2$

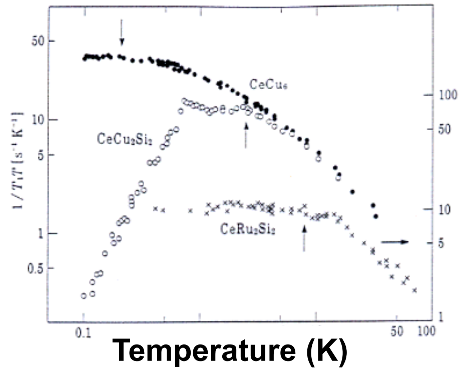

6-12図 $CeCu_6$, $CeCu_2Si_2$, $CeRu_2Si_2$ の $(T_1T)^{-1}$ の温度依存性 (Y

Coherence effect in resistivity ρ(T) due to Ce periodic lattice

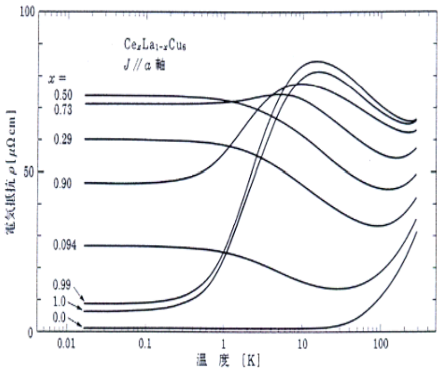

Temperature (K)

Magnetic and transport behaviors in various Ce ($4f^1$) compounds

Magnetic susceptibility

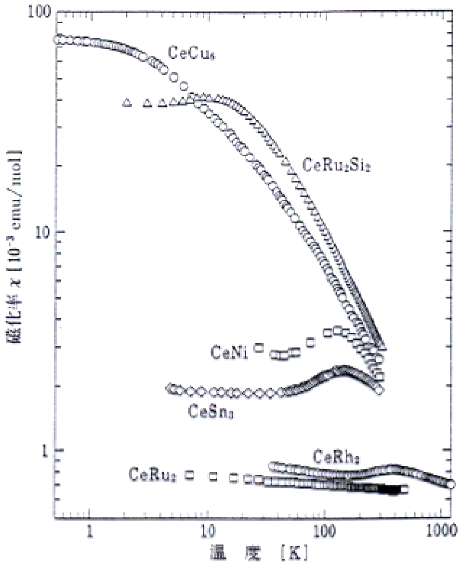

Resistance

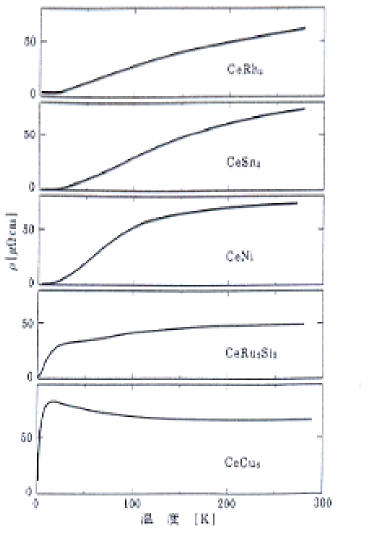

磁気秩序をもたない Ce 化合物の電気抵抗の温度依存性

	T_c(K)	crystal structure	nucleus	$1/T_1$	K^*	parity	symmetry
CeCu$_2$Si$_2$[17,22–25]	~ 0.7 K	tetragonal(ThCr$_2$Si$_2$)	Cu, Si[26,27]	T^3	decrease	even	*d*
CeCoIn$_5$[20,21]	~ 2.3 K	tetragonal(HoCoGa$_5$)	Co, In[28]	T^3	decrease	even	*d*
CeIrIn$_5$[20,21]	~ 0.4 K	tetragonal(HoCoGa$_5$)	In[29]	T^3	-	-	-
UBe$_{13}$[18,19]	~ 0.9 K	cubic(NaZn$_{13}$)	Be[30]	T^3	-	-	-
UPt$_3$[18,19]	~ 0.55 K	hexagonal	Pt[31–34]	T^3	unchange	odd	*p* or *f*
URu$_2$Si$_2$[18,19]	~ 1.2 K	tetragonal(ThCr$_2$Si$_2$)	Ru, Si[35,36]	T^3	unchange	odd	
UNi$_2$Al$_3$[18,19]	~ 1 K	hexagonal	Al[37]	T^3	unchange	odd	*p* or *f*
UPd$_2$Al$_3$[18,19]	~ 2 K	hexagonal	Pd, Al[38,39]	T^3	decrease	even	*d*
CeCu$_2$Ge$_2$[40]	~ 0.6 K (P ~7.6 GPa)	tetragonal(ThCr$_2$Si$_2$)	-	-	-	-	-
CeIn$_3$[41–45]	~ 0.2 K (P ~2.5 GPa)	cubic(AuCu$_3$)	In[46]	T^3	-	-	-
CePd$_2$Si$_2$[41,42,47]	~ 0.4 K (P ~2.5 GPa)	tetragonal(ThCr$_2$Si$_2$)	-	-	-	-	-
CeRh$_2$Si$_2$[48,49]	~ 0.2 K (P ~1.0 GPa)	tetragonal(ThCr$_2$Si$_2$)	-	-	-	-	-
CeRhIn$_5$[50,51]	~ 2.1 K (P ~1.6 GPa)	tetragonal(HoCoGa$_5$)	In[52,53]	T^3	-	-	-
High-T_c cuprates	~ 140 K (max)	perovskite	Cu, O	T^3	decrease	even	*d*
Sr$_2$RuO$_4$[54,55]	~ 1.5 K	perovskite	Ru, O	T^3	unchange	odd	*p*

Table I. Superconducting characteristics in most heavy-fermion systems along with high-T_c cupper oxides and Sr$_2$RuO$_4$. Note that the nuclear relaxation rate $1/T_1$ reveals no coherence peak just below T_c, followed by the T^3 dependence without an exception. K^* denotes the spin component of Knight shift below T_c. In this context, all unconventional superconductors discovered to date possess the line-node gap on the Fermi surface regardless of either spin-singlet *d* wave or spin-triplet *p*-wave.

Reference : JPSJ, 74 (2005) 186-199."Unconventional SC in HFs"

Signature of Heavy Effective Mass

Resistivity 電気抵抗

"Kondo lattice"

ρ $\mu\Omega\cdot$cm

$\rho=\rho_0+AT^2$

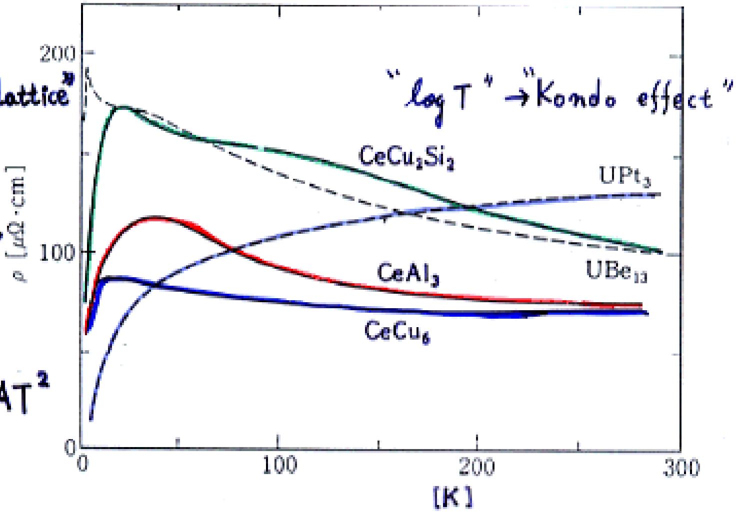

$A\propto\gamma^2$

Specific Heat 比熱

$C=\gamma T$

電子比熱係数

$\frac{C}{T}$

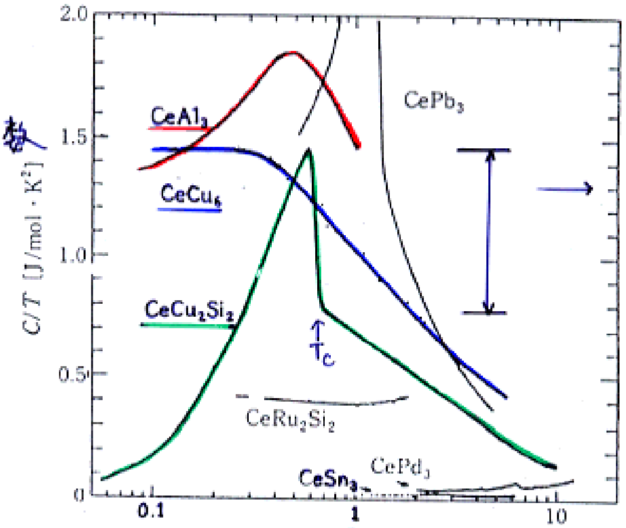

$\rightarrow$ $\frac{\Delta C}{\gamma T_c}\simeq 1.2$

$C/T=\underset{\sim}{\gamma_e}+\beta T^2+\ldots$

1979 Steglich et al.

Superconductivity

Conventional superconductivity:

Cooper pair

attractive interaction: electron-phonon coupling

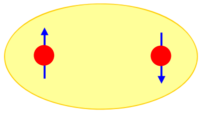

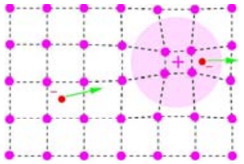

s-wave spin singlet

pairing channel: angular momentum l=0 and spin s=0

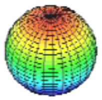

order parameter: $\Psi(\vec{r})=\left|\Psi(\vec{r})\right|e^{i\phi(\vec{r})}$

broken symmetry: U(1) gauge $\rightarrow$
- Meissner-Ochsenfeld-effect (Higgs)
- persistent currents
- flux quantization

Symmetry of Cooper Pairs

Pair wavefunction: $F_{ss'}(\vec{k}) = \langle \hat{c}_{\vec{k}s} \hat{c}_{-\vec{k}s'} \rangle = \underbrace{\Phi(\vec{k})}_{\text{orbital}} \underbrace{\chi(s,s')}_{\text{spin}}$

totally antisymmetric under electron exchange

$$\vec{k} \to -\vec{k} \qquad s \leftrightarrow s'$$

even parity
L = 0, 2, 4, ...
$\Phi(-\vec{k}) = \Phi(\vec{k})$ → S=0 singlet

odd parity
L = 1 ,3 ,5, ...
$\Phi(-\vec{k}) = -\Phi(\vec{k})$ → S=1 triplet

Magnetic fluctuations mediated SC mechanism

Ferromagnetic case

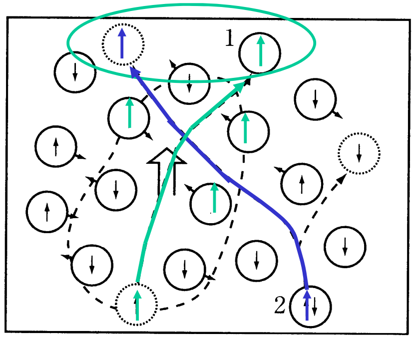

Antiferromagnetic case

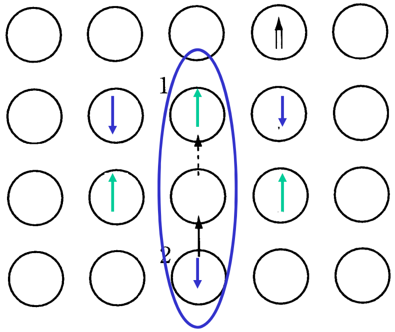

Various types of SC pairing states

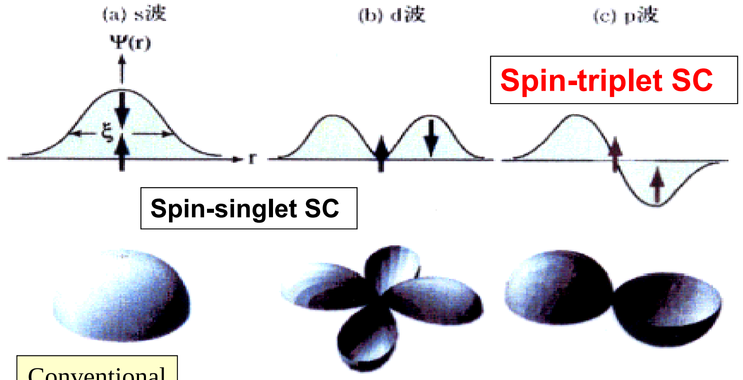

Spin-triplet SC

Spin-singlet SC

Conventional SC

Copper oxides high-T_c SC

Heavy- electrons SC

UPt_3, Sr_2RuO_4 UNi_2Al_3

Energy gap structure of unconventional SC

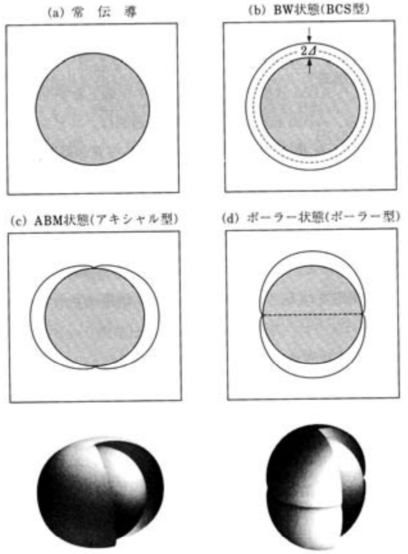

7-3図　BW，ABM，ポーラー状態に対するエネルギーギャップの様子

Phase diagrams of AFM and SC in HFS

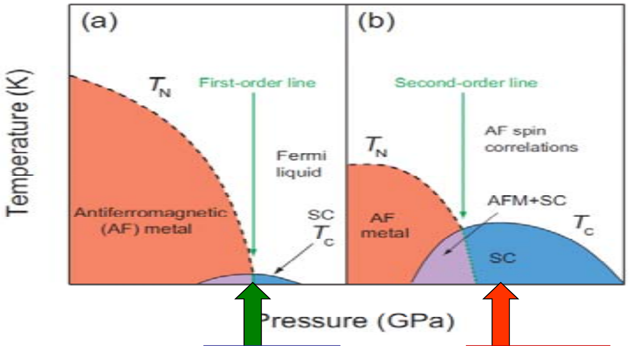

Materials	AFM	T_c (P:GPa)
$CeRh_2Si_2$	AF : T_N=36 K	0.4 K (0.9)
$CePd_2Si_2$	AF : T_N=10 K	0.4 K (2.2)
$CeNi_2Ge_2$	Critical	0.2 K (2.3)
$CeCu_2$	AF : T_N=3.5 K	0.15K (5.9)
$CeIn_3$	AF : T_N=10 K	0.2 K (2.4)

Materials	T_c(P:GPa)	AFM
$CeCu_2Si_2$	0.6 K (P=0)	Critical
$CeIrSi_3$	1.6 K (2.6)	AF : T_N=4.2 K
$CeRhIn_5$	2.1 K (2.1)	AF : T_N=3.8 K
$CeCoIn_5$	2.3 K (P=0)	Critical

$CeIn_3$

S. Kawasaki et. al .

Phys. Rev. B, 77, 064508 (2008)

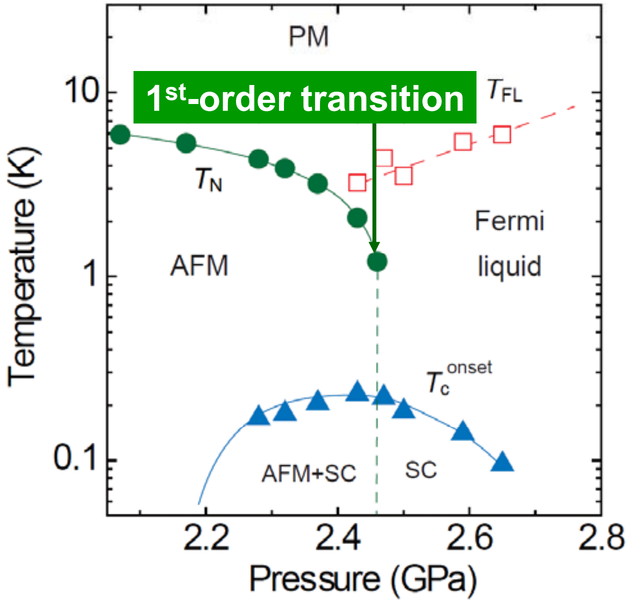

Correlation between Magnetic Structure and Onset of SC

$CeRhIn_5$

M. Yashima et al .

Phys. Rev. B **79**, 214528 (2009).

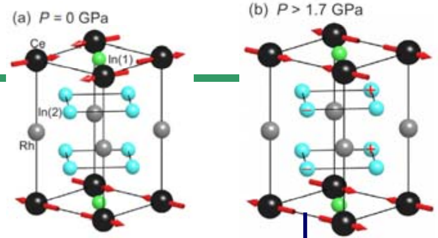

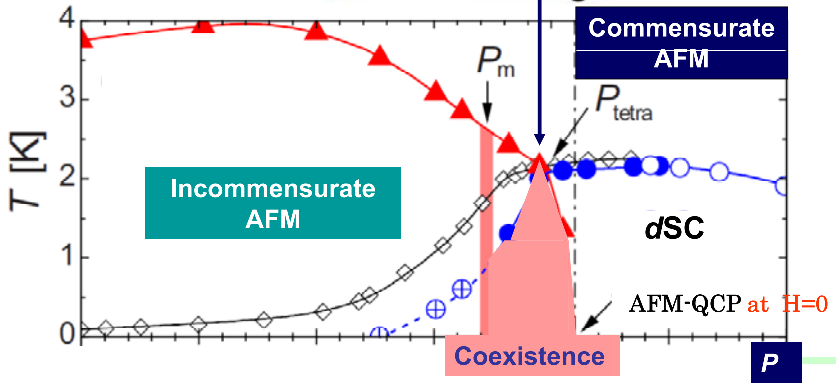

Coexisting phases of AFM and SC

Ferromagnet UGe_2

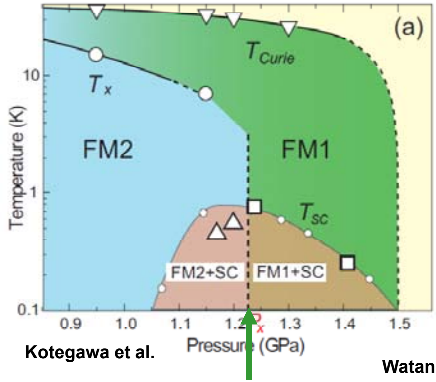

Kotegawa et al.

1st-order transition

Watanabe & Miyake et al.

Antiferromagnet $CeNiGe_3$

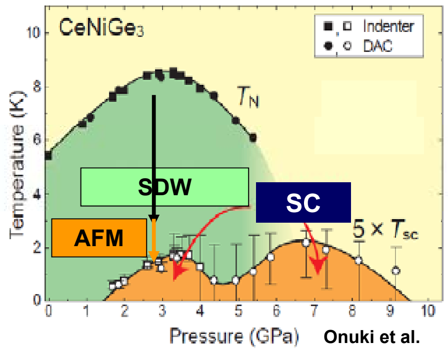

Onuki et al.

Harada et al.

Longitudinal fluctuations of ordered moments mediate Cooper pairs ?

Variation of phase diagrams in heavy-electrons systems

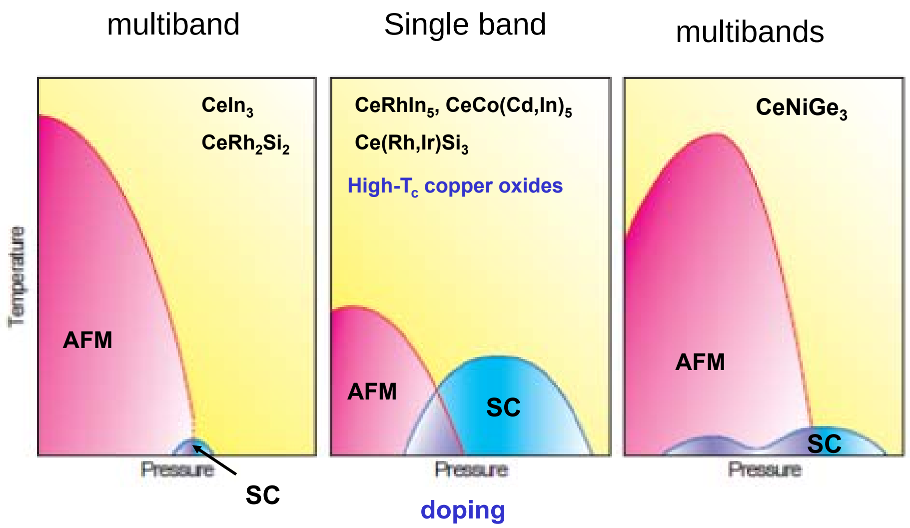

Phase Diagram

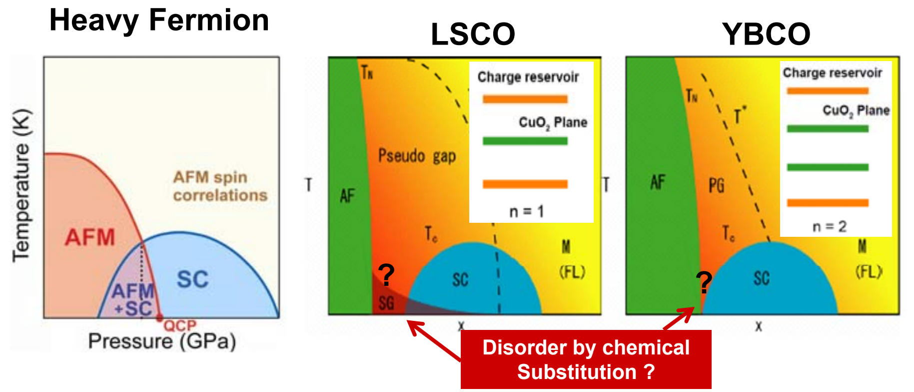

AFM order can coexist with *d*SC

A number of CuO$_2$ layers dependence of Phase Diagram ?

→AFM and SC compete or coexist ? in high-T$_c$ cuprates

Hg-based multilayered systems

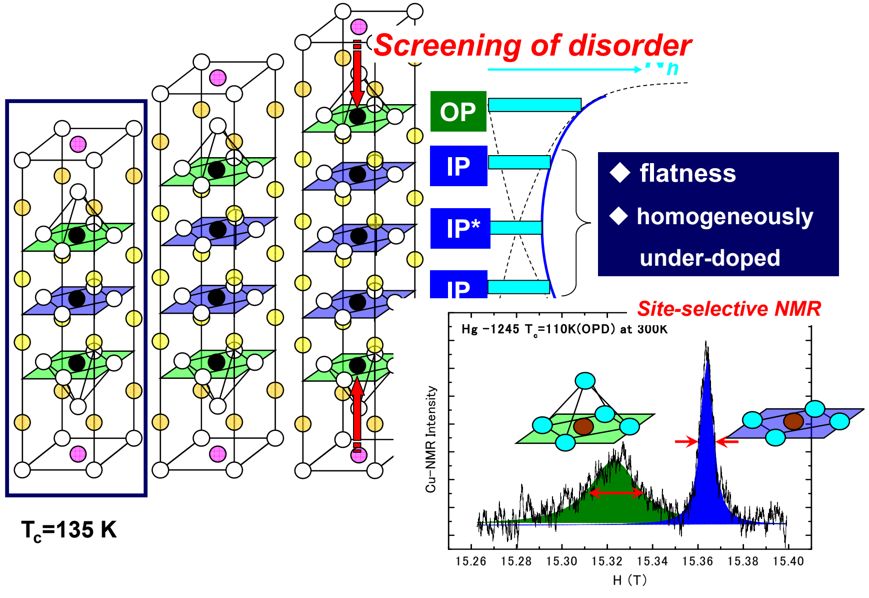

- flatness
- homogeneously under-doped

T$_c$=135 K

The n=5 (Hg,Tl,Cu) compounds

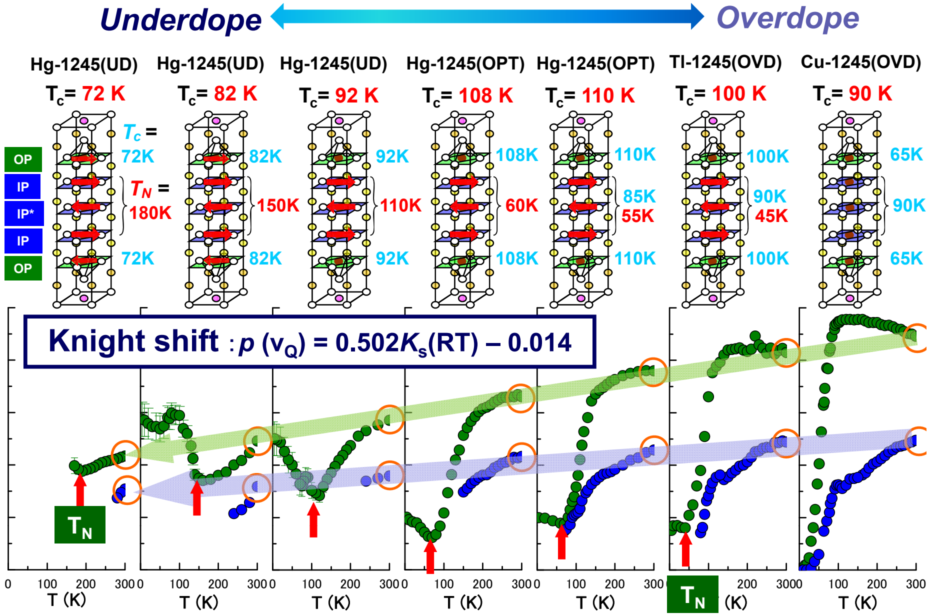

Knight shift : $p\ (\nu_Q) = 0.502K_s(\mathrm{RT}) - 0.014$

The n=5 compounds ~phase diagram~

$(Hg,Tl,Cu)Ba_2Ca_4Cu_5O_{10+\delta}$

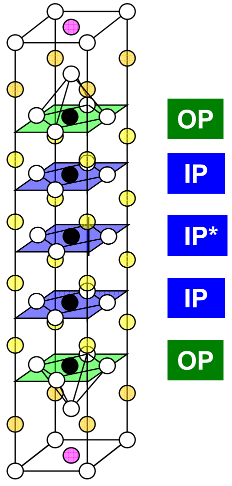

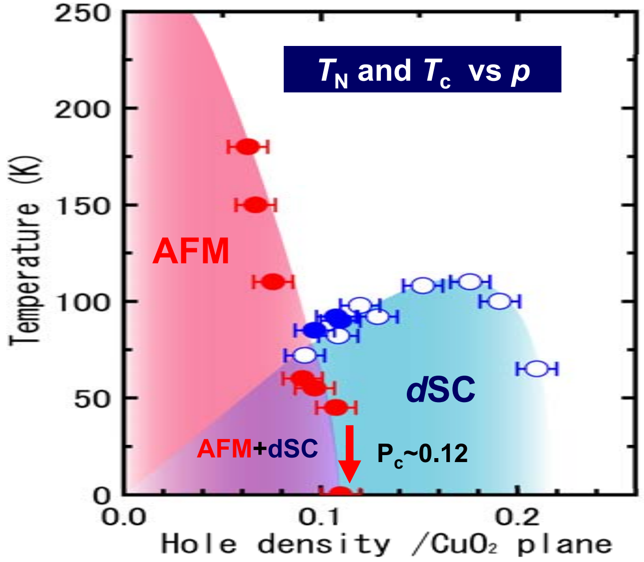

Multilayered Systems with Apical Fluorine (F^{-1})

O^{2-} substitution for F^{-1} dopes holes carriers

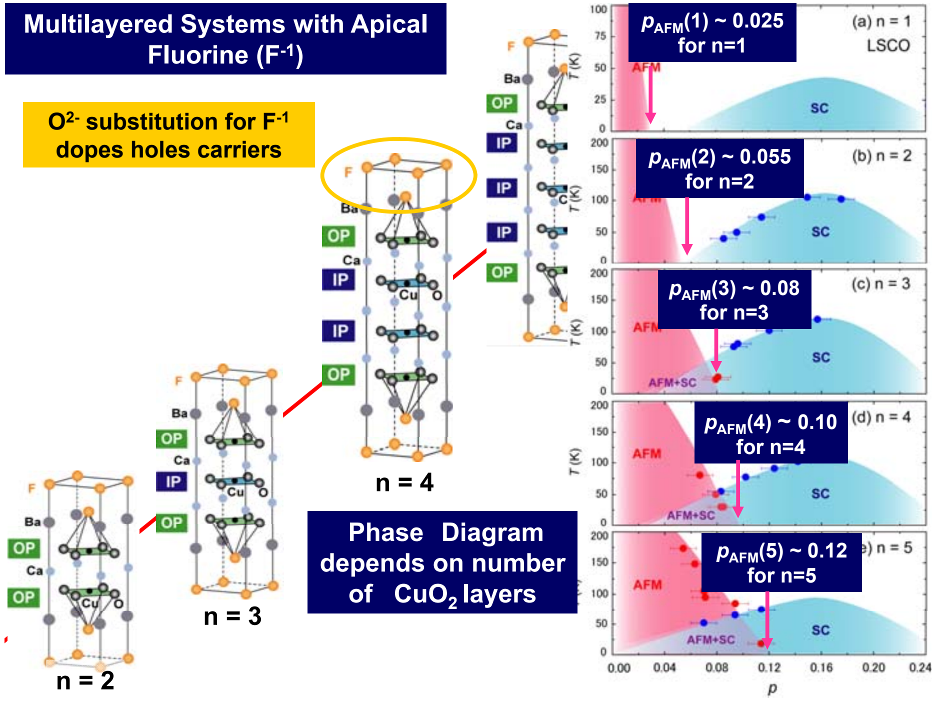

Phase Diagram depends on number of CuO_2 layers

Microscopic evidence for *AFM* + dSC from ^{19}F-NMR

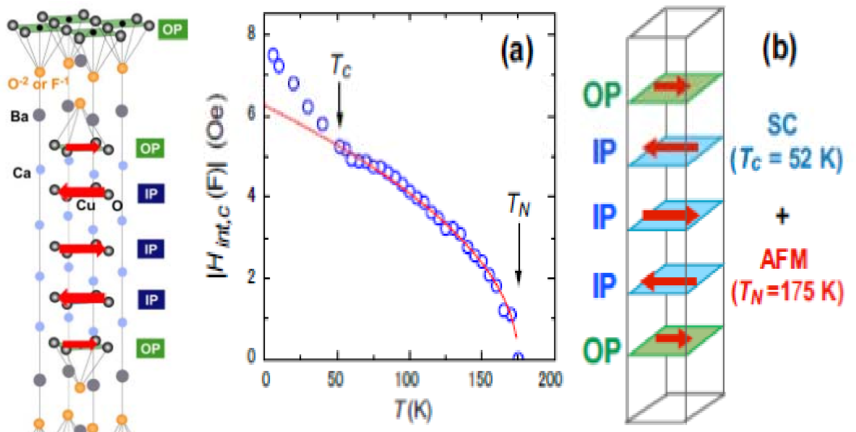

T_N = 175 K + T_c = 52 K

Coexistence of AFM and dSC

Energy gap probed by ARPES on n = 4 compounds

Chen, et al., PRL 97 (2006)

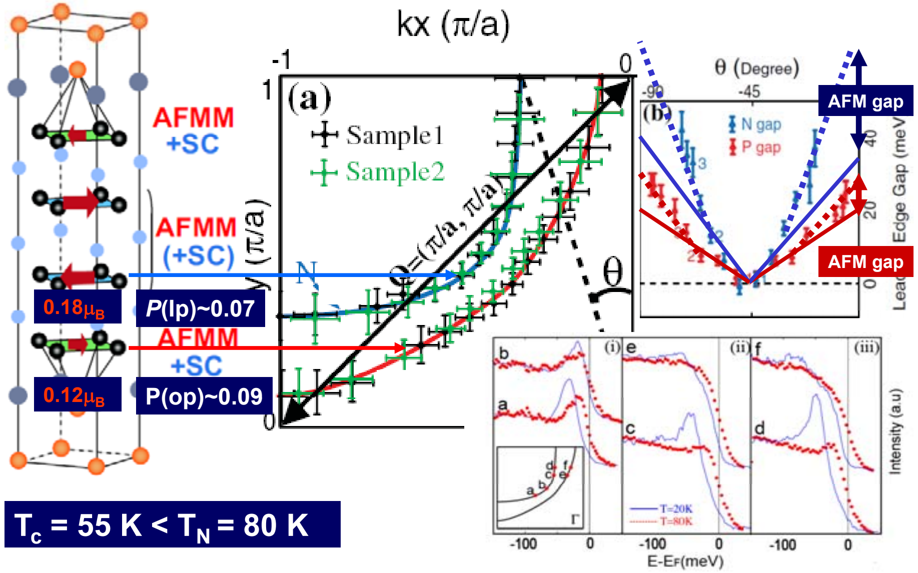

T_c = 55 K < T_N = 80 K

ARPES : Evidence for two-gap behaviors in underdoped regime

Tri-layer $Bi_2Sr_2Ca_2Cu_3O_{10+y}$ **Bi-layer $Bi_2Sr_2CaCu_2O_{8+y}$**

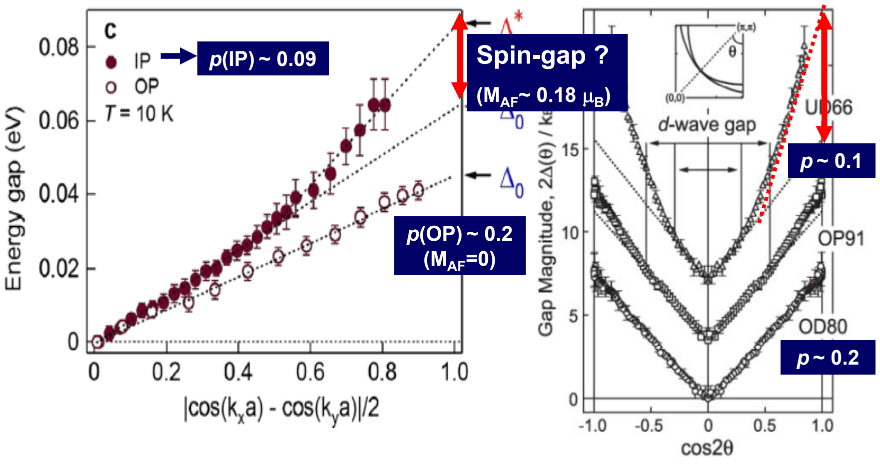

S. Ideta et al., PRL 104, 227001 (2010)

T. Anzai et al (2010)

Experiment : Phase Diagram of M_{AF} and Δ_{SC} *vs* *p* *at* 1.5 K

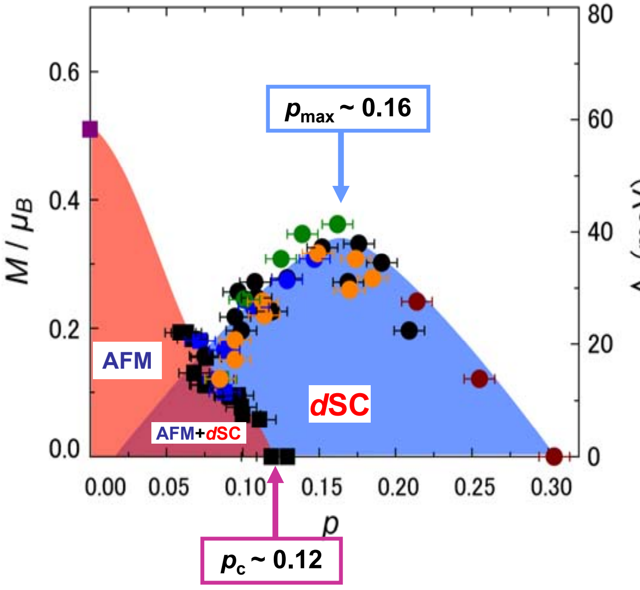

	M	Δ
n=∞	■	
n=5	■	●
n=4	■	●
n=3	■	●
n=2		●
n=1		●

n=2 : 0212F, also

$YBa_2Cu_3O_{6.6}$, $YBa_2Cu_3O_7$, $YBa_2Cu_4O_8$, $Bi_2Sr_2CaCu_2O_8$

n=1 : Tl-2201

T=0 Phase Diagram (Theory) : Comparison with Experiment

High-T_c oxides: Strong correlation regime of U/t

Mott Insulator

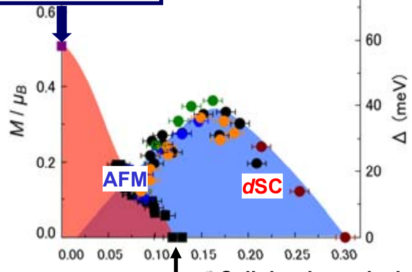

PRL **96**, 087001 (2006)
PRL **98**, 257001 (2007)
JPSJ **77**, 124706 (2008)
JPSJ **78**, 064705 (2009)
PRB **79**, 064505 (2009)

Variational Monte Carlo on the t – J model

S. Pathak et al., PRL 102, 027002 (2009)

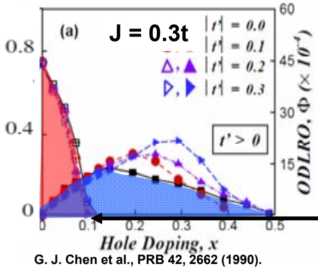

G. J. Chen et al., PRB 42, 2662 (1990).
T. Giamarchi et al., PRB 43, 12 943(1991).
A. Himeda and M. Ogata, PRB 60, R9935 (1999).
T.K. Lee and C.T. Shih, PRB 55, 5983(1997).

P_c~0.12

Cellular dynamical mean-field theory (C-DMFT) on the Hubbard model

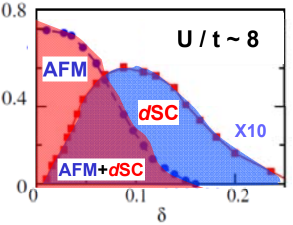

M. Capone and G. Kotliar, PRB 74, 054513 (2006).
D. Senechal et al. ,PRL 94, 156404 (2005).

Summary for HTSC

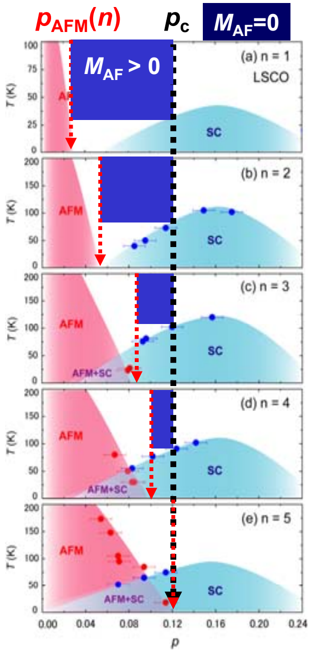

Quantum and Thermal Fluctuations suppress the onset of static AFM order and hence may cause fluctuations of SC order parameter's amplitude and phase

Phase diagram of M_{AF} and Δ_{dSC} at Low T

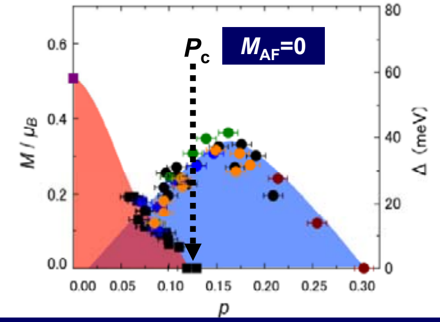

***Mott physics*: The large AFM exchange coupling *J* is the origin for HTSC raising T_c as high as 160 K, and there are no bosonic glues.**

Origin of force in the Nature

Magnetic exchange interaction

$-JS_1 \cdot S_2$

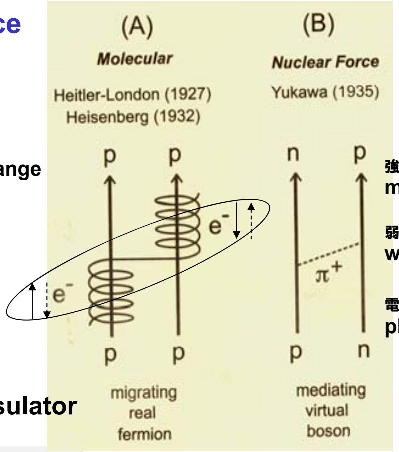

強い相互作用：meson

弱い相互作用：weak bosons

電磁相互作用：photon

Formation of Copper pairs

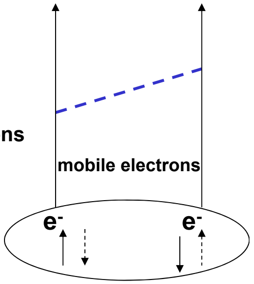

BCS theory :

Mediating virtual bosons: phonon

magnetic excitations

AFM Mott Insulator

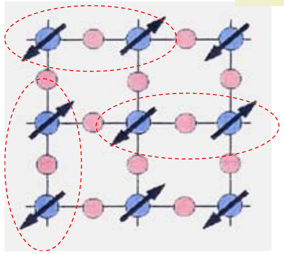

Heisenberg Model

$$H = \sum_{\langle i,j \rangle} J_{ij} \boldsymbol{S}_i \cdot \boldsymbol{S}_j,$$

AFM + Local Spin Singlet

T=0 Phase Diagram : Comparison with the Calculations

Carrier doping

$$H = \sum_{\langle i,j \rangle} t_{ij} a^{\dagger}_{i\sigma} a_{j\sigma} + \sum_{i} J_{ij} \boldsymbol{S}_i \cdot \boldsymbol{S}_j$$

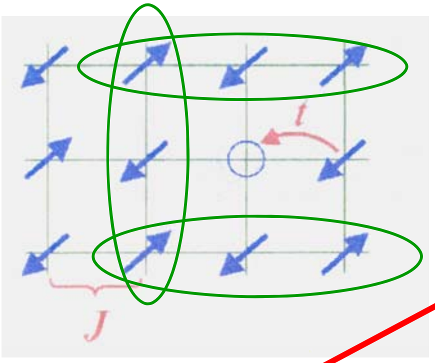

Variational Monte Carlo on the t – J model

S. Pathak et al., PRL 102, 027002 (2009)

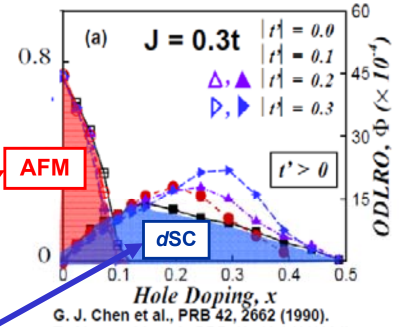

G. J. Chen et al., PRB 42, 2662 (1990).
T. Giamarchi et al., PRB 43, 12 943(1991).
A. Himeda and M. Ogata, PRB 60, R9935 (1999).
T.K. Lee and C.T. Shih, Phys. Rev. B 55 (1997) 5983.

Suppression of AFM

+ mobile spin-singlet pairs

Summary of this talk

	CuO_2 systems	HFS
Mother compound	AFM-Mott Insulators with $T_N \sim 500$ K	Antiferromagnets Ferromagnets Multiple orders
Phase diagram	Carrier doping	Pressure Chemical substitution
Electronic state	Single band	Multibands
SC order parameter	d-wave $T_c = 135$ K	d-wave, odd parity (triplet), non-unitary, hybrid-type, extend s-wave
Attractive interaction	AFM Interaction	Magnetic (density) fluctuations, Valence ones, Quadruple ones, Magnetic excitons, Multiple scattering effect due to on-site U